Wind and Structures, Vol. 8, No. 6 (2005) 427-442
DOI: http://dx.doi.org/10.12989/was.2005.8.6.427

Numerical and wind tunnel simulation of pollutant dispersion in the near wake of buildings

X. Wang and K.F. McNamara†

Department of Civil Engineering, National University of Ireland, Galway, Ireland
(Received September 8, 2003, Revised June 29, 2004, Accepted May 2, 2005)

Abstract. Numerical and wind tunnel simulations of pollutant dispersion around rectangular obstacles with five aspect ratios have been conducted in order to identify the effects of flow patterns induced by buildings on plume dispersion in the near wake of buildings. An emission from a low source located upwind of obstacles was used in this simulation. The local flow patterns and concentrations around a cubical obstacle were initially investigated using three RANS turbulence models, (the standard k-ε, Shear Stress Transport (SST), Reynolds-Stress RSM turbulence model) and also using Large-eddy simulation (LES). The computed concentrations were compared with those measured in the wind tunnel. Among the three turbulence models, the SST model offered the best performance and thus was used in further investigations. The results show, for normal aspect ratios of width to height, that concentrations in the near wake are appreciably affected because of plume capture by the horseshoe vortex and convection by the vertical vortex pairs. These effects are less important for high aspect ratios. Vertical vortex pairs present a strong ability to exchange mass vertically and acts efficiently to reduce ground-level concentrations in the near wake.

Keywords: dispersion; building effects; horseshoe vortex; vertical vortex pairs; near wake.

1. Introduction

Pollutant dispersion in the near wake of buildings depends mainly on two mechanisms, i.e., transportation by the organized flow and diffusion by turbulence. It is known that the local flow pattern and turbulence characteristics around buildings are very complicated. Flows are significantly influenced by flow separation and reattachment, horseshoe vortex, roof and sidewall trailing vortices and flow recirculation. This leads to the concentration fields around buildings being significantly affected by these local flow patterns, especially when sources are located close to buildings. To model pollutant dispersion in the near wake, it is necessary to examine each local flow pattern individually and quantify the effects of each flow pattern on pollutant dispersion, then determine which flow pattern dominates the plume dispersion, or determine the fraction of each flow pattern and then use weighed averages of their effects.

Flow recirculation in the near wake was considered as the main local flow pattern adopted in some state-of-the-art building downwash algorithms, e.g., PRIME and ADMS (Robins, *et al*. 1997, Schulman, *et al*. 2000). It is presumed in these models that the recirculating flow make the pollutant

† Professor, Corresponding Author, E-mail: Kevin.mcnamara@nuigalway.ie

uniformly mixed, thus the box model or the modified box model may apply in either the whole of the near wake or in its alongwind direction. Wind tunnel and field measurements have shown that such building downwash algorithms only present a limited resolution in the near wake, e.g., for an isolated rectangular building the differences between the experimental values and estimated ones for the ground-level concentration are usually out by a factor of 1.5~2.0 (Robins, *et al*. 1997). The difference rises to a factor of 10 if a plume is close to the building. This shows that these building downwash models are somewhat crude in predicting concentrations in the near wake.

Wind tunnel experiments of the flow field around isolated rectangular obstacles in a neutral boundary layer have been carried out by Becker and co-workers (Becker, *et al*. 2002). Their results, mainly for a building width-to-height ratio, $W/H=2$, identify that the vertical vortex pairs are one of the most important local flow patterns in the near wake. The flow topographies they gave show that the local flow pattern in the near wake has similar horizontal structure, i.e., flow streamlines which pass around the sidewalls and over the roof will be trapped into the vertical vortex pairs. Mavroidis and co-workers (Mavroidis and Griffiths 2001, Mavroidis, *et al*. 2003) conducted a series of field and wind tunnel investigations for both isolated and clusters of obstacles with different shape and aspect ratios for a near upwind source. They found that these vertical vortex pairs present a strong ability for vertical mass exchange. The vertical vortex pairs carry pollutants vertically up to the top of an obstacle, thus the ground level concentrations become lower inversely proportional to the height of the obstacle. These physical and numerical simulations supply very useful information on pollutant dispersion in the near wake. However they provide little information about the effects of building aspect ratios on the local flow patterns and on the concentration field in the near wake.

In this paper an investigation, combining computational simulations with wind tunnel trials, has been conducted for isolated rectangular obstacles with five aspect ratios to obtain details of the flow field and the concentration field in the near wake. This investigation focuses on the effects of plume capture by the horseshoe vortex and the effects of the vertical vortex pairs on pollutant dispersion in the near wake. In section 2 the case details are described. The schemes for wind tunnel experimentation and CFD calculations are presented in section 3 and section 4, respectively. Results from computational simulations and wind tunnel trials are analyzed and discussed in section 5 and section 6. The corresponding conclusions are given in section 7.

2. Case details

As shown in Table 1 rectangular obstacles with five aspect ratios were used in this simulation. They represent buildings with a regular aspect ratio, a wide building, a tall building and a long building, respectively. A stack was placed upwind of the tested obstacle at a distance of double

Table 1 Geometrical detail of model obstacles

Case	$H \times W \times L$ (cm)	W/H	L/H	h_s/D
1	$10\times10\times10$	1.0	1.0	0.5
2	$10\times20\times10$	2.0	1.0	0.5
3	$10\times60\times10$	6.0	1.0	0.5
4	$10\times10\times20$	1.0	2.0	0.5
5	$30\times10\times10$	1/3	1/3	0.5

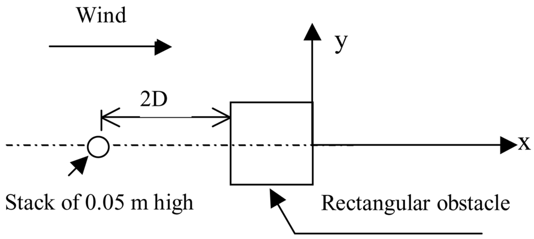

Fig. 1 Model setup and the coordinate system

the minimum dimension of the projected area of the obstacle in the alongwind direction. The setup of the models and the coordinate system used in this simulation are shown in Fig. 1. In the figure and the table, H is the obstacle height, W is obstacle width and L is obstacle alongwind length. D is the minimum dimension of the alongwind projected area, i.e., $D = \min(H, W)$ and h_s is the stack height.

3. Wind tunnel experiment

The wind tunnel experiment was conducted in the boundary layer wind tunnel at NUI, Galway. This is a low speed, open-return and open working section type wind tunnel. The test section is 1.99 m high and 2.44 m wide and the overall length of the wind tunnel is 15.75 m. The wind speed range is 0 to 7 m/sec. Using Irwin-spires, perforated strip and roughness elements with a staggered arrangement a wind-tunnel boundary layer was modelled, which at the experimental site was about 1.0 m thick, the roughness length z_0 was 1.27 mm and the exponent of the power-law velocity profile was 0.256. Based on detailed flow measurements and a comparison with ESDU full-scale data, (ESDU 1982, 1983, 1985), the boundary layer represents the roughness terrain for the center of small town at a scale factor of 1:250. The same scaling factor was used for the relationship between prototypes and models in both the wind tunnel experiments and the numerical simulation. Typically, the model dimensions for Case 1 represents a cubical building of 25 m height.

In the wind tunnel experiment ethane tracer gas was delivered to the model stack at a constant rate of 0.3 L/min via a flowmeter. A Pitot tube was located in front of the test obstacle at a height of 1.0 m. The mean velocity at this altitude was set to 5.0 m/s and thus the reference wind velocity, U_{ref}, was 2.66 m/s at the reference height of $H_{ref} = 0.1$ m. The friction velocity, u^*, was estimated by fitting the logarithmic law giving a value of 0.245 m/s. The minimum Reynolds number based on the minimum dimension of the alongwind projected area of the obstacle was about 1.8×10^4, which is above the critical Reynolds number 11,000 to ensure a turbulence flow pattern (ASCE 1996).

Concentration samples were analysed by a M200 Micro Gas Chromatograph (GC). Samples were collected from various locations using 1mm brass taps fitted either on either a rake or on the raised wind tunnel floor. Plastic tubes were attached to each of the brass taps and connected to a port of a Scanivalve. A user-developed program was used to automatically move the Scanivalve one port forward when a sample had been analysed by the GC. An air pump, which was installed close to the sample inlet of the GC, was used to draw and feed gaseous samples to the inlet of the GC. In this way concentration samples were continuously acquired and analysed by one GC. The corresponding chromatograms and concentration quantities were recorded using a PC.

Measured concentrations are expressed as dimensionless χ-values which is defined as:

$$\chi = CU_{ref}H_{ref}^2/Q \tag{1}$$

where U_{ref} and H_{ref} are the reference wind velocity and reference height as described, Q is the emission rate and C is the concentrations from the GC. It is worth noting that C-values were obtained in terms of the ensemble average of 3 runs. This is based on the fact that the concentration values from the GC correspond to an average time of only 0.1 second, which is the injection time of the GC. This ensemble averaging was expected to average out some of the concentration fluctuations from large eddies.

Based on the requirements of ensemble averaging, the sampling processes were designed as a series of sampling sessions under the same conditions. At the start of each sampling session, a first 5-min period was allowed to ensure the flow field to stabilize and another 5-min to allow the concentration field to stabilize. Background concentrations were measured at the start and end of each sampling session and subtracted from the measured data by presuming that they vary linearly with time.

4. Numerical simulation

The commercially available CFD code, CFX5.6, was used for the numerical simulations and run on the SGI parallel mainframe at NUI, Galway. The numerical simulation consists of two stages: Case 1 (see Table 1) was run using three RANS turbulence models, i.e., the standard k-ε, Shear Stress Transport (SST) and Reynolds-stress (RSM) models, respectively. The results were compared with wind tunnel experiments and published experimental data. The turbulence model with best accuracy was selected for investigation of other cases. Large Eddy Simulation (LES) was also conducted for Case 1 to provide detailed flow patterns around the cube.

The computational domain was selected as $H_d \times W_d \times L_d = 1.2 \times 1.9 \times 3.4$ m. Identical mesh grids were used for both the RANS calculations and the LES calculation in order to cancel the effects of mesh resolutions. Surface mesh controls were applied to all solid surfaces. Inflation elements were used in near wall regions. Typically, the mesh size is 1 mm thick near solid surfaces and the maximum length is 45 mm. Solution convergence was controlled by two criteria: 1) the normalised root mean square residuals were below 1.0×10^{-4} and 2) the global imbalance was below 5% for all variables.

4.1. RANS run

The inlet conditions used in the standard k-ε and the SST models were determined by a combination of measured mean velocity and turbulence intensity profiles with scaled ESDU full-scale data (ESDU 1983, 1985). They are given by:

$$U(z) = U_{ref}(z/H_{ref})^{\alpha}, \quad k = 0.5(\sigma_u^2 + \sigma_v^2 + \sigma_w^2), \quad \text{and} \quad \varepsilon = (u_*)^3/(\kappa z), \tag{2}$$

where parameters $\kappa = 0.4$, $u_* = 0.245$ m/s, U_{ref} and H_{ref} are defined previously and σ_u, σ_v and σ_w are the standard deviations of the fluctuating components u, v and w, respectively. The profiles of turbulence kinetic energy, k, and turbulence dissipation rate, ε, are shown in Fig. 2.

For the RSM model, the profiles of mean flow, isotropic Reynolds stress components, $\overline{u'_i u'_i}$ and ε in the inlet are identical to Eq. (2). The anisotropic Reynolds stress components, $\overline{u'_i u'_j}$ $(i \neq j)$, are

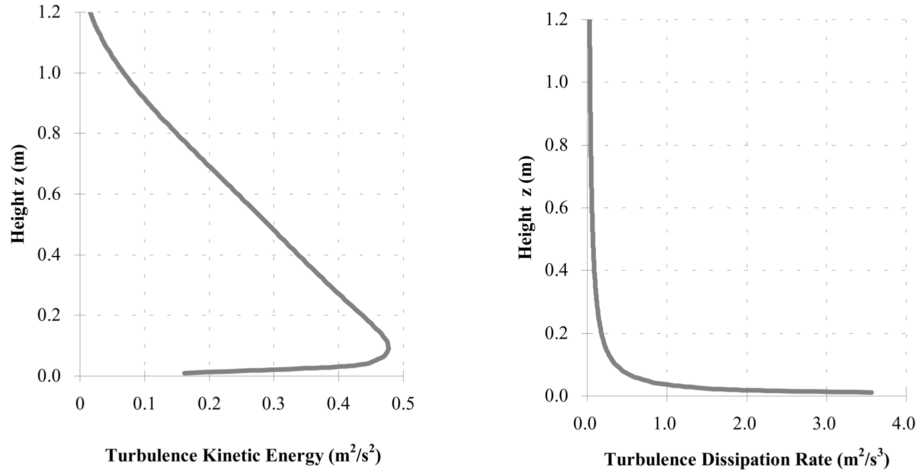

Fig. 2 Profiles of k and ε for the inlet boundary condition

approximated by:

$$\overline{u'w'} = -u_*^2(1-z/\delta)^2 \text{ and } \overline{u'v'} = \overline{v'w'} = 0 \quad (3)$$

where δ is the boundary layer thickness and the expression for $\overline{u'w'}$ is from ESDU (1985).

Other boundary conditions used in the computational domain are as follows: zero gradient condition for the outlet, symmetry planes for both lateral surfaces and the upper surface and no slide smooth wall conditions for all solid surfaces.

4.2. LES run

The mean wind profile used in the LES run was the same as for the RANS run. The inlet turbulence was approximated by superimposing random fluctuations on the mean velocity components. The fluctuating velocity components were assumed to obey a Gaussian distribution whose standard deviation was determined by the measured turbulence intensity profile and the empirical expressions given by ESDU (1983). The random number method was used to generate the turbulence with the specified turbulence statistics. Other boundary conditions applied on the computational domain are: zero gradient condition for the outlet, free-slip wall for both lateral surfaces and the upper surface and no slide smooth wall conditions for all solid surfaces.

5. Results and discussions

5.1. Assessment of turbulence models

The flow patterns around a cube are characterised by the reattachment lengths defined in Fig. 3. Comparisons of computed reattachment lengths from the three turbulence models and the LES run with available experimental data are summarized in Table 2. It should be noted that the computational reattachment lengths were estimated from the streamwise velocity values at the points nearest to the walls. It is obvious that LES results agree very well with experimental values

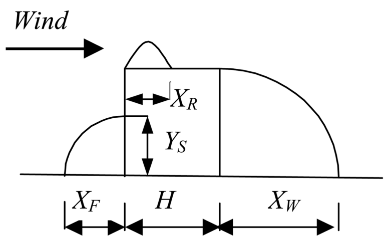

Fig. 3 Definition of reattachment lengths around a cube

Table 2 Summary of mean separation and reattachment lengths around cube

Model	X_F/H	Y_S/H	X_R/H	X_W/H
Standard k-ε	0.47	0.79	> 1.0	1.80
SST	0.77	0.74	0.36	2.28
RSM (SSG)	0.24	0.69	0.37	2.21
LES (SGS)	1.01	0.84	0.90	1.46
Exp. (Hoxey, *et al.* 2002)	0.75	0.58	0.57	1.4
Exp. (Shah and Ferziger 1997)	1.02		0.7	1.2

in all reattachment lengths. The three RANS turbulence models exhibited almost identical abilities to predict the stagnation point on the windward wall but predicted different reattachment lengths otherwise. The standard k-ε model predicted the wake reattachment length well but gave a relatively small upwind ground separation distance. It also failed to predict roof-top flow separation. The SST turbulence model predicted roof-top flow separation well and also upwind separation distance but tends to over-predict the wake reattachment length. The RSM model predicted roof-top reattachment length well but significantly under-predicted the upwind ground separation distance and over predicted the wake reattachment length.

Comparisons of the computed concentrations with measured ones in the wind tunnel are given in three profiles in the wake:

1) alongwind profile at the centreline and $z/H_{ref}=0.5$ (Fig. 4a),
2) lateral profile at ground level and $x/H_{ref}=0.5$ (Fig. 4b), and
3) vertical profile at the centerline and $x/H_{ref}=0.5$ (Fig. 4c).

The three RANS turbulence models tend to under-predict the magnitude of the mean concentration in the near wake due to the fact that they usually under-estimated the turbulent diffusion caused by larger eddies. They agree well with wind tunnel results further downwind as the larger eddies are broken down into smaller eddies with downwind distance. This also means that in the near wake the plume width is generally narrower than that observed in the wind tunnel (see Fig. 4b). Comparatively, the SST model predicted a more favourable concentration distribution in the near wake even though it predicted a relatively long wake reattachment length compared with the wind tunnel observations. Therefore the SST turbulence model was used in further case investigations.

5.2. Flow fields around an isolated obstacle

Fig. 5 and Fig. 6 give the local flow patterns around a cube from the LES run. The horseshoe vortex, lateral vortices, the roof-top vortex, and the two recirculation vortices can be seen around

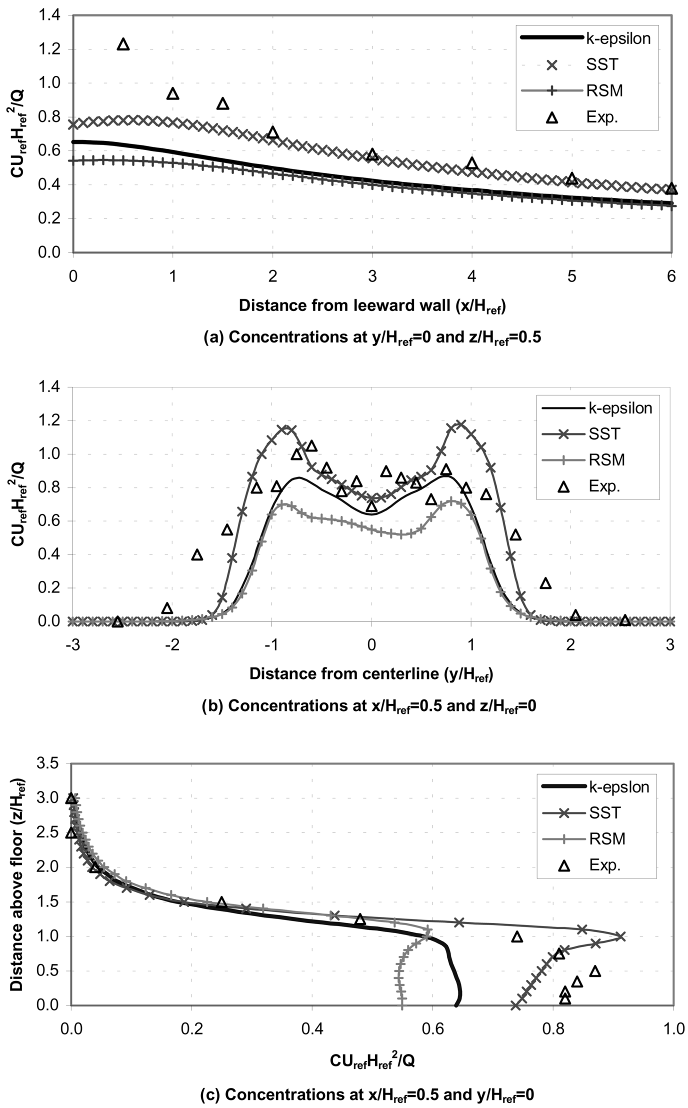

Fig. 4 Comparison of computed with measured concentrations for the cube case

the cube. The two corner vortices behind the cube join at the symmetry plane and form an arch. This agrees very well with the wind tunnel experiments (Martinuzzi and Tropea 1993).

When a pollutant is emitted from an upwind low level source near buildings the concentration field in the near wake may be closely linked with all the above flow patterns. The plume may be captured and transported by the horseshoe vortex to the wake or simply pass around the roof-level and sidewall to enter the wake. In other words, the concentration distribution is very sensitive to source location relative to the obstacle. Therefore, an investigation of the evolution of these flow patterns is important to understand the wake concentration field.

Fig. 7 shows that the approaching flow from different ‘seeds’ may be developed into a number of flow patterns around a cubic obstacle. Streamline “seeds” were arranged within a small circular

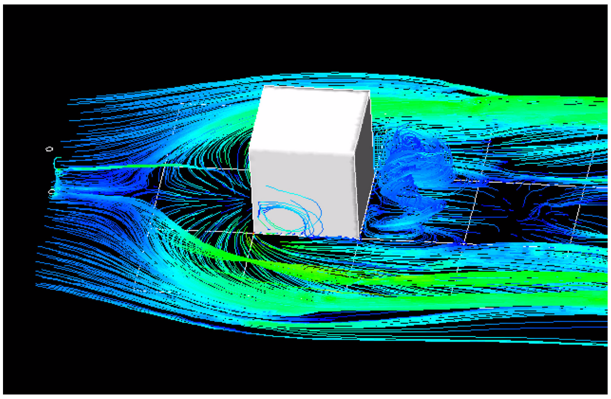

Fig. 5 Streamlines of mean flow around a cube on the ground (LES)

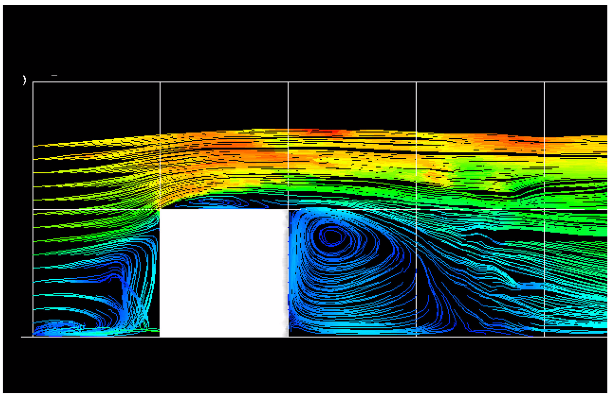

Fig. 6 Streamlines of mean flow around a cube on the center plane (LES)

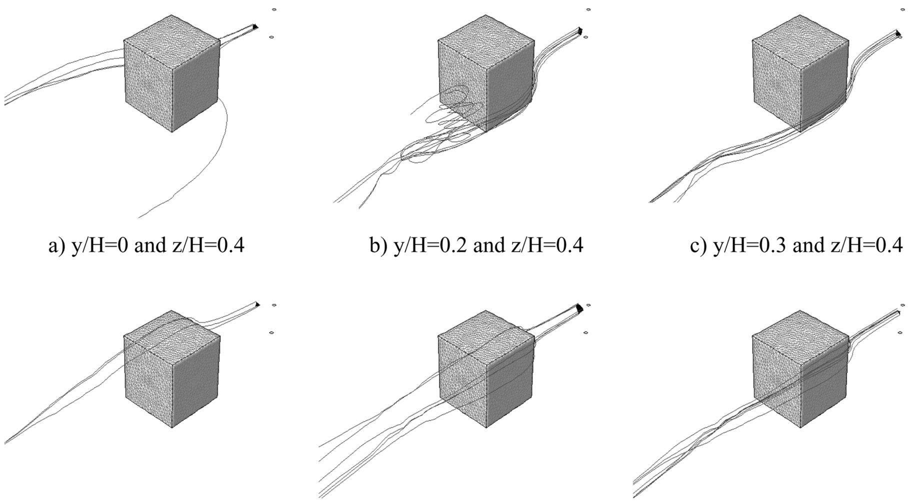

a) y/H=0 and z/H=0.4 b) y/H=0.2 and z/H=0.4 c) y/H=0.3 and z/H=0.4

d) y/H=0 and z/H=0.7 e) y/H=0.2 and z/H=0.7 f) y/H=0.3 and z/H=0.7

Fig. 7 Streamline plots for the cube case (LES), the sub-labels refer to the locations of streamline “seeds” plane normal to the approaching flow and were located upwind of the cube by 1.5H. By moving this circular plane at either a given height or a given crosswind distance, the resultant streamlines can provide insights on the evolution of these flow patterns around the obstacle. It is seen that above the stagnation point the approaching flow goes over the roof and/or passes around the sidewalls. Below the stagnation point the approaching flow rolls down to the ground and forms the horseshoe vortex. It was noted that when "seeds" were located between 0.2H to 0.3H and within a crosswind distance of 0.1H to 0.2H part of the streamlines diverge from the horseshoe vortex at a downwind distance of about 1.0H and develop into a pair of inward counter-rotating vertical vortices. Theoretically the generation and development of both the horseshoe vortex and the wake vertical vortex pairs may be interpreted from the pressure field around the cubical obstacle. Ahead of the windward wall the outward-rotating standing-vortices are formed by the negative pressure gradient toward the sidewalls and towards the ground. The interaction of these vortices with the ground and sidewalls leads to them being stretched further and intensified. Finally parts of the vortices with relatively higher curvature are trapped into the near wake due to the negative pressure gradient. This shows that the greatest effect of the horseshoe vortex on the concentrations in the near wake corresponds to a source which is away from the centreline.

The aspect ratio of rectangular obstacles affects the flow patterns around the obstacle as well as the strength and generation of the vertical vortex pairs. For tower-like obstacles with an aspect ratio of $W/H = 1/3$, as shown in Fig. 8, the wake vertical vortex pairs and lateral vortices are significantly

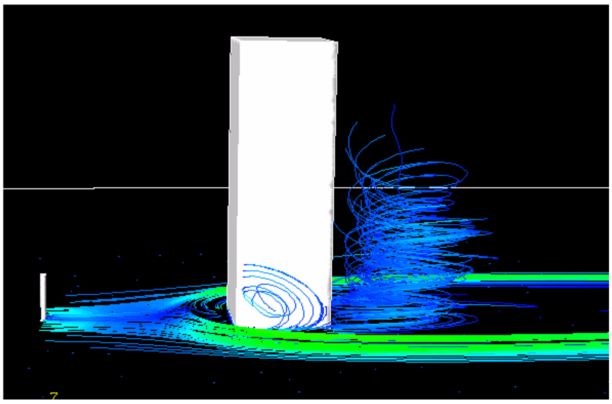

Fig. 8 Streamline plot for an aspect ratio of $W/H = 1/3$ (SST)

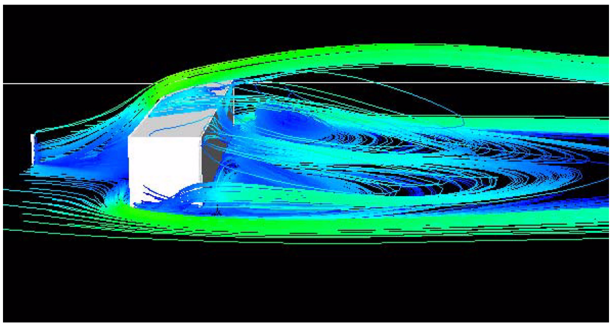

Fig. 9 Streamline plot for an aspect ratio of $W/H = 6$ (SST)

stronger than those observed for the cube case. However for a wide obstacle with an aspect ratio of $W/H=6.0$, as shown in Fig. 9, flow in the vicinity of the centerline approximates to a two-dimensional flow pattern. The vortices formed at the front of the lower middle-span of the windward wall tend to stand parallel because of the small lateral pressure gradient and immediately move down and back, finally they converge into the main flow over the roof. The vertical vortex pairs in the wake are located only at the corners of the leeward wall. The near wake flow in the middle part is dominated by the roof-level separation.

Further numerical investigations were conducted for an obstacle with an aspect ratio of $W/H=2.0$ and $L/H=2.0$. Compared with the cube case, both the horseshoe vortex and the vertical vortex pairs get stronger as the aspect ratio W/H rises to 2.0 but become weaker as the aspect ratio L/H rises to 2.0. A possible explanation is that streamlines have high curvature for high aspect ratios of width-to-height so that they can diverge from the horseshoe vortex and be entrained into the near wake. Inversely, increasing the aspect ratio L/H results in the streamline curvature becoming lower around the sidewalls, thus less streamlines diverge into the near wake.

5.3. Concentration field in the near wake

Fig. 10 shows the computed concentration contours for the cube case. The maximum ground-level concentration around the obstacle follows the footprint of the horseshoe vortex (Fig. 10b). This demonstrates that the horseshoe vortex carries the plume around the sidewalls so that the ground-level concentration around the obstacle is dominated by this mechanism. This also leads to the lateral profile of ground-level concentration having two peaks.

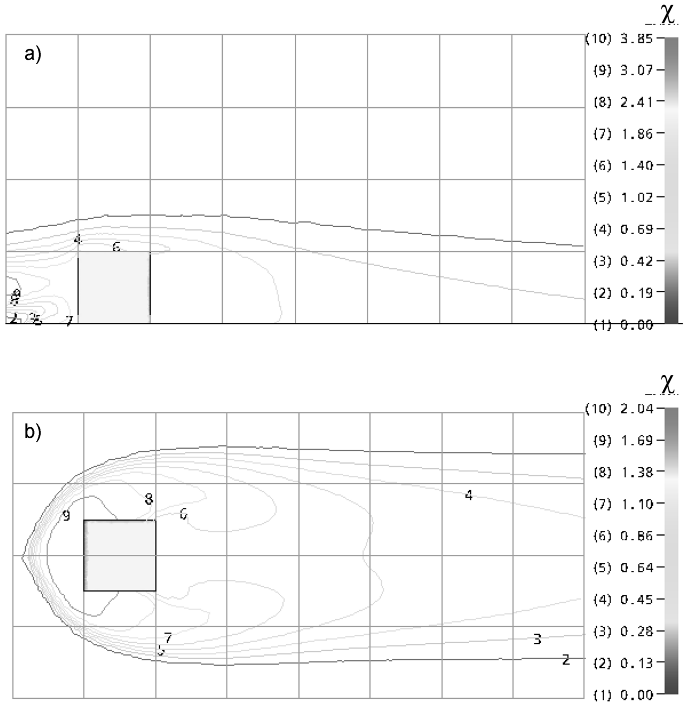

Fig. 10 Concentration contours for the cube case at: a) the centerline plane and b) the ground plane (SST)

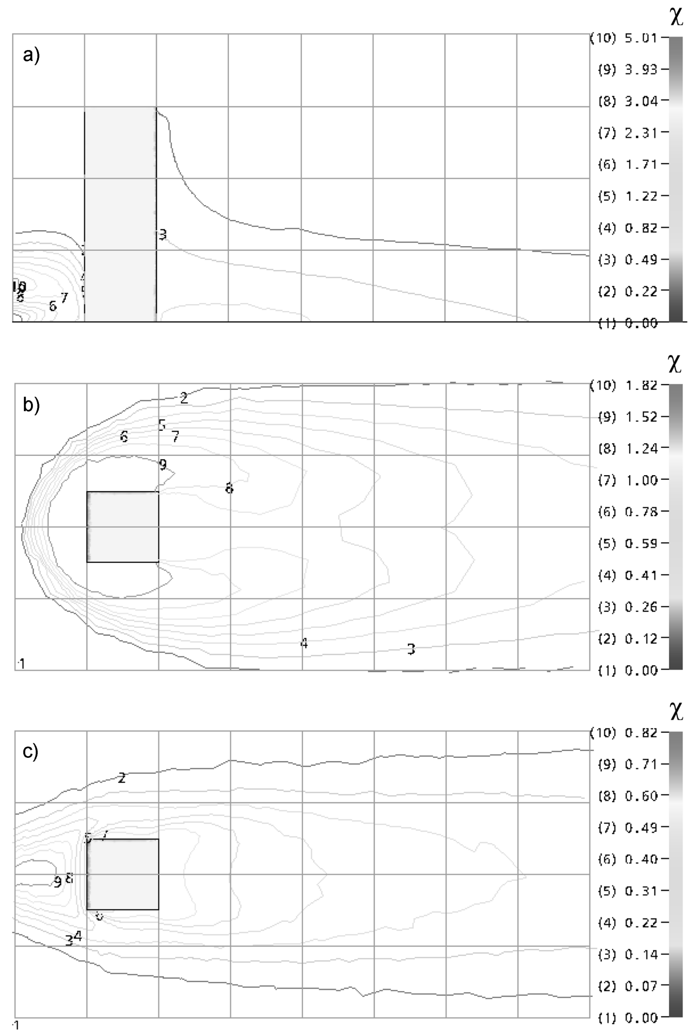

Fig. 11 Concentration contours for Case 5 ($W/H = 1/3$, $W=L$) at: a) the centerline plane, b) the ground plane and c) the plane at $z/H = 1/3$ (SST)

For a tower-like obstacle with an aspect ratio of $W/H = 1/3$, the plume can not pass over the roof and thus is influenced much more by the horseshoe vortex. In this situation, the plume dispersion in the near wake is dominated by both the horseshoe vortex and vertical vortex pairs. It is obvious from Fig. 11 that the vertical dimension of the plume in the near wake increases substantially in comparison to that in front of the windward wall. It shows that there exists significant vertical mass exchange in the near wake. As a result, the ground level concentrations in the near wake become lower when compared with the cube case.

As shown in Fig. 9, for an aspect ratio of $W/H = 6$ the approach flow onto the lower part of the middle-span of the windward wall will immediately pass over the roof instead of being entrained into the horseshoe vortex. This means that the horseshoe vortex is less effective in transporting the plume into the near wake because the plume scale is relatively small compared with the obstacle

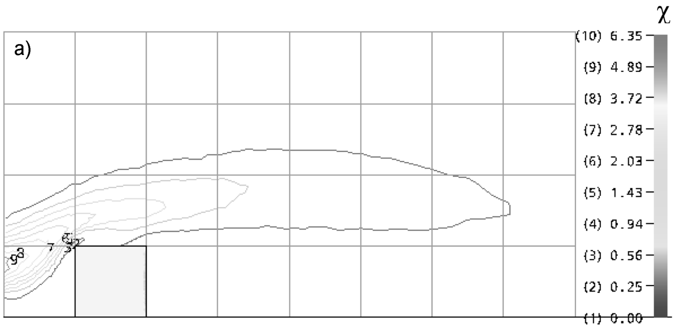

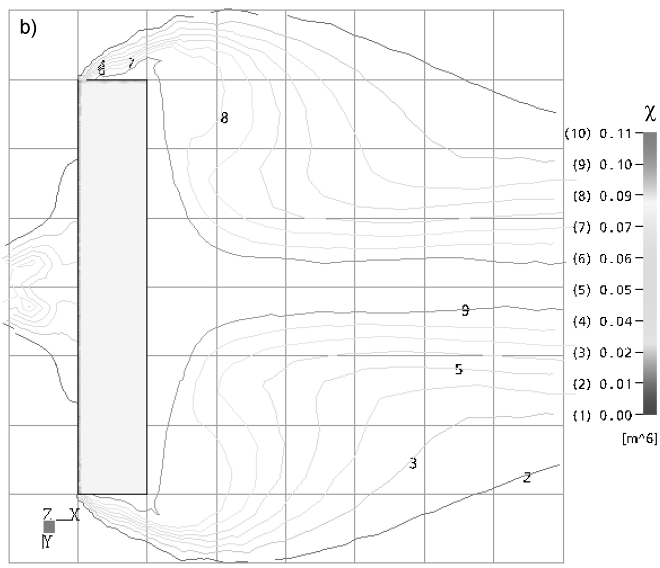

Fig. 12 Concentration contours for Case 3 ($W/H=6$, $H=L$) at: a) the centerline plane and b) the ground plane (SST)

width. The plume is mainly carried over the roof by the mean flow. This can be seen in Fig. 12 where the concentration level in the near wake is relatively low. On the other hand, it may be observed that in the near wake the lateral width of the plume become very wide and is approximately uniform in the crosswind direction when close to ground. This shows that the vertical vortex pairs transport the plume laterally.

The measured concentration profiles are shown in Fig. 13. These concentrations measured in the wind tunnel present the same trend as the computed results. Fig. 13 implies that near wake concentrations may depend on three factors: the fraction of plume captured by the horseshoe vortex, the distance of the footprint of the horseshoe vortex away from the centerline and the influences of vertical vortex pairs.

Fig. 13(a) shows that the ground-level concentrations at x/H=0.5 decrease quickly with aspect ratio W/H. Due to identical upwind low source configurations a wider obstacle increases the lateral blockage so that a greater fraction of the plume passes over the roof and less plume is captured by the horseshoe vortex. This leads to relatively low ground-level concentrations in the near wake.

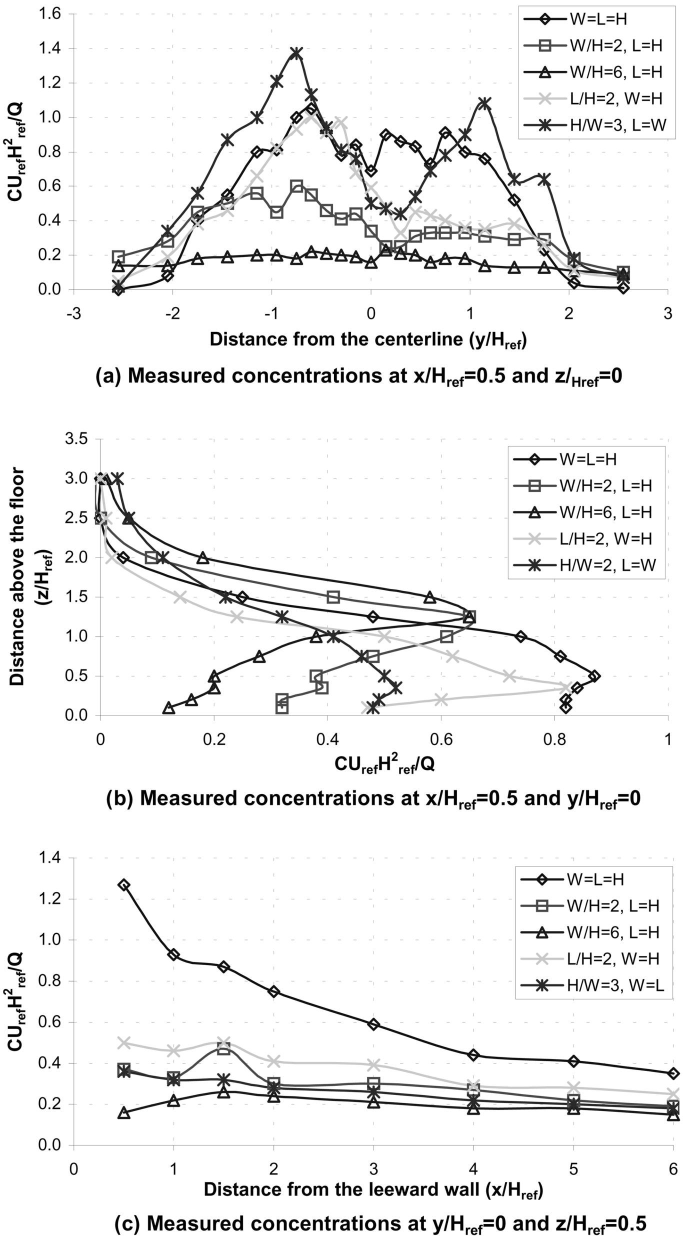

Fig. 13 Measured concentration profiles for five aspect ratios

When the aspect ratio of *H/W* is increased the ground-level concentrations at $x/H=0.5$ increase. This seems to show that an increasing fraction of the plume is captured by the horseshoe vortex. It is also observed that the aspect ratio *L/H* tends to decrease the ground-level concentrations at $x/H=0.5$ but the influence is much smaller relative to the aspect ratio *W/H*. When compared with the cube case, higher aspect ratios of *H/W* lead to more plume being captured by the horseshoe vortices but concentrations behind the obstacle are relatively low because the distance between the two legs of the horseshoe vortices become wider. Higher *H/W* aspect ratios also lead to lower ground level concentrations because of increased vertical mixing.

Fig. 13(b) shows that when pollutants in the near wake come mainly from the fraction captured by the horseshoe vortex, for example Case 1 and Case 4, the vertical spreading of pollutants in the near wake depends mainly on the vertical mass transport by the vertical vortex pairs. This leads to vertical concentration profiles becoming relatively uniform below the roof level. The vertical concentration profiles will approximate the Gaussian distribution when pollutants in the near wake come mainly from the top of the near wake, for example Case 2 and Case 3.

The variation of obstacle aspect ratio causes some differences in the alongwind concentration profiles, as shown in Fig. 13(c). The centerline concentrations at $z/H_{ref}=0.5$ shows a reduction in the near wake when close to the leeward wall for a very wide obstacle. This implies that pollutants enter the near wake mainly from the top of the near wake.

6. Further discussion

As shown in Section 5.1, the three RANS turbulence models reproduced the qualitative nature of both the local flow patterns and the concentration distribution around a cubical obstacle. However the SST model predicted the quantitative results better because it predicted the upwind cavity length best and thus the fraction of the plume captured by the horseshoe vortex. Further comparisons of CFD simulation with wind tunnel measurements show that the quantitative results are significantly affected by building aspect ratios. For example, the SST model tends to under-predict the plume rise for larger building width-to-height ratios and thus may significantly over-predict the near wake concentration close to the ground for very wide obstacles (Wang 2004). This suggests that the selection of the RANS turbulence models is strongly case-dependent. For a successful CFD simulation it is very important to reproduce the most critical flow patterns which dominate a dispersion process.

Section 5.2 shows that the formation of vertical vortex pairs is related to the divergence of unstable eddies in the horseshoe vortex to some extent. This seems to link the approaching flow within a region which is below the stagnation point on the windward wall and deviates somewhat with distance from the centreline (see Fig. 7). This implies that the peak value of near wake concentrations could become relatively higher when a source is located within this region. However, this was not investigated in this simulation and therefore further investigations are needed to validate it.

Section 5.3 shows the bifurcation of the plume in the wake and two peaks appear on the lateral near wake concentration profiles for an obstacle with regular aspect ratios. Plume bifurcation behind a rectangular obstacle was also observed in wind tunnel and field investigations and was attributed to the effects of the horseshoe vortex (e.g. Macdonald, *et al*. 1998) and (Mavroidis and Griffiths 2002). A double Gaussian distribution was suggested to fit this non-Gaussian lateral concentration profile by Macdonald and co-workers (Macdonald, *et al*. 1998). The wind tunnel measurements in this simulation show that the plume bifurcation in the wake may disappear for a very wide building. Furthermore, detailed CFD simulations show that such a bifurcation of the lateral concentration profile decays with height and recovers to the Gaussian distribution at roof level (Wang 2004). This is somewhat different from the observations in a field investigation carried out by Mavroidis and Griffiths (2002), their results show that the bifurcation of the lateral profiles still exist, to some extent, at roof level. These differences should be investigated further.

7. Conclusions

Numerical and wind tunnel simulations of pollutant dispersion around rectangular obstacles with five aspect ratios have been conducted for an emission from a low level source located upwind of the obstacles. The results have shown that building aspect ratios have a significant influence on concentration distribution in the near wake:

(1) The portion of the plume captured by the horseshoe vortex dominates the near wake concentration field for smaller width-to-height ratios. This causes relatively higher ground-level concentrations and the lateral concentration profile was bifurcated in the near wake.

(2) The plume was elevated for larger building width-to-height ratios and a smaller fraction of the plume was captured by the horseshoe vortex. This reduces the ground-level concentrations and diminishes the bifurcation of the lateral concentration profile. The bifurcation of the lateral concentration profile disappears for very wide buildings. As a result, the ground-level concentrations become significantly lower when compared with the cube case.

(3) Although an increase in either the obstacle width or height decreases the ground-level concentrations in the near wake, the obstacle width has a much greater effect.

(4) The vertical vortex pairs in the near wake have a strong influence on the vertical and lateral mass exchange. For tower-like buildings this yields significantly lower ground-level concentrations. For a wide building the concentration distribution tends to be uniform laterally.

By comparison with wind tunnel experiments all three RANS turbulence models, (the standard k-ε, SST and RSM models), show good ability to predict the qualitative nature of the near wake concentration. However, they predicted slightly less diffusivity and may either under-predict or over-predict the magnitude of concentrations in the near wake. When the horseshoe vortex dominates the plume dispersion the SST turbulence model reproduced more realistic concentrations in the near wake than either the standard $k-\varepsilon$ or the RSM turbulence model. However, for a very wide building the SST model may under-predict the ground-level concentrations due to the over-prediction of plume rise.

Acknowledgements

This work is sponsored by a grant from the HEA of Ireland No: ECI: WA-3. The authors would like to thank the National Centre for Biomedical Engineering Science at NUI, Galway, for providing the computational resources for this study.

References

ASCE (1996), “Wind-tunnel studies of buildings and structures”, *J. Aerospace Eng.,* **9**(1), 19-36.

Becker, S., Lienhart, H. and Durst, F. (2002), “Flow around three-dimensional obstacles in boundary layers”, *J. Wind Eng. Ind. Aerodyn.,* **90**, 265-279.

ESDU (1982), “Strong winds in the atmospheric boundary layer. Part 1: mean-hourly wind speeds”, ESDU item No. 82026.

ESDU (1983), “Strong winds in the atmospheric boundary layer. Part 2: discrete gust speeds”, Item No. 83045.

ESDU (1985), “Characteristics of atmospheric turbulence near the ground, Part II: single point data for strong winds (neutral atmosphere)”, ESDU item No. 85020.

Hoxey, R. P., Richards, P. J. and Short, J. L. (2002), “A 6 m cube in an atmospheric boundary layer flow Part 1. Full-scale and wind-tunnel results”, *Wind and Struct.,* **5**(2~4), 165-176.

Martinuzzi, R. and Tropea, C. (1993), “The flow around surface-mounted prismatic obstacle placed in a fully developed channel flow”, *J. Fluids Eng*., **115**, 85-92.

Macdonald, R.W., Griffiths, R.F. and Hall, D.J. (1998), “A comparison of results from scaled field and wind tunnel modelling of dispersion in arrays of obstacles”, *Atmospheric Environment*, **32**(22), 3845-3862.

Mavroidis, I. and Griffiths, R.F. (2002), “Comparison of open-path and point measurements of a gaseous pollutant in the vicinity of a model building”, *Water, Air, and Soil Pollution: Focus*, **2**(5&6), 655-667.

Mavroidis, I. and Griffiths, R.F. (2001), “Local characteristics of atmospheric dispersion within building arrays”, *Atmospheric Environment*, **35**, 2941-2954.

Mavroidis, I., Griffiths, R.F. and Hall, D.J. (2003), “Field and wind tunnel investigations of plume dispersion around single surface obstacles”, *Atmospheric Environment* **37**, 2903-2918.

Robins, A., Carruthers, D. and McHugh, C. (1997), “The ADMS building effects module”, *Int. J. Environ. Pollution*, **8**(3-6), 708-717.

Schulman, L.L., Strimaitis, D.G. and Scire, J.S. (2000), “Development and evaluation of the PRIME plume rise and building downwash model”, *J. Air & Waste Management Association,* **50**, 378-390.

Shah, K.B. and Ferziger, J.H. (1997), “A fluid mechanicians view of wind engineering: Large eddy simulation of flow past a cubic obstacle”, *J. Wind Eng. Ind. Aerodyn.,* **67&68**, 211-224.

Wang, X. (2004), “Numerical and wind tunnel simulations of building effects on pollutant dispersion”, Ph.D. thesis, Dept of Civil Engineering, National University of Ireland, Galway.

CC